

## Formation of analogs of cometary nitrogen-rich refractory organics from thermal degradation of tholin and HCN polymer



Jean-Yves Bonnet<sup>a,b,1</sup>, Eric Quirico<sup>a,b,\*</sup>, Arnaud Buch<sup>c</sup>, Roland Thissen<sup>a,b</sup>, Cyril Szopa<sup>d,e</sup>, Nathalie Carrasco<sup>d,e,f</sup>, Guy Cernogora<sup>d,e</sup>, Nicolas Fray<sup>g</sup>, Hervé Cottin<sup>g</sup>, Lena Le Roy<sup>g</sup>, Gilles Montagnac<sup>h</sup>, Emmanuel Dartois<sup>i</sup>, Rosario Brunetto<sup>i</sup>, Cécile Engrand<sup>j</sup>, Jean Duprat<sup>j</sup>

<sup>a</sup> Univ. Grenoble Alpes, IPAG, F-38000 Grenoble, France

<sup>b</sup> CNRS, IPAG, F-38000 Grenoble, France

<sup>c</sup> Ecole Centrale de Paris, Chatenay Malabry, France

<sup>d</sup> Université Versailles St-Quentin, Sorbonne Universités, UPMC Univ., Paris 06, France

<sup>e</sup> CNRS/INSU, LATMOS-IPSL, Guyancourt F-78280, France

<sup>f</sup> Institut Universitaire de France, Paris F-75005, France

<sup>g</sup> LIISA, UMR 7583 du CNRS, Université Paris-Est Créteil, Université Paris-Diderot, Créteil, France

<sup>h</sup> Ecole Normale Supérieure de Lyon, Université Claude Bernard, CNRS, LGLTPE, 69364 Lyon Cedex 07, France

<sup>i</sup> Institut d'Astrophysique Spatiale (IAS), Université Paris-Sud, UMR 8617-CNRS INSU, Bât 121, F-91405 Orsay, France

<sup>j</sup> Centre de Sciences Nucléaires et de Spectrométrie de Masse (CSNSM), Université Paris-Sud, UMR 8609-CNRS/IN2P3, F-91405 Orsay, France

### ARTICLE INFO

#### Article history:

Received 20 May 2014

Revised 2 October 2014

Accepted 4 November 2014

Available online 27 November 2014

#### Keywords:

Cosmochemistry

Organic chemistry

Solar Nebula

Comets

Interplanetary dust

### ABSTRACT

Nitrogen-rich refractory organics are scarce phases recovered as a fraction of stratospheric IDPs and constitute the bulk of the organic matter of some ultracarbonaceous Antarctic micrometeorites. They are likely formed under very specific conditions within a nitrogen-rich environment and may provide valuable clues on the origin of the population of interplanetary dusts accreted by Earth. In this study, we produced relevant analogs of such refractory organics characterized in three ultracarbonaceous Antarctic micrometeorites, starting from the carbonization of an HCN polymer and a tholin. Indeed, carbonization is a process that can increase the polyaromatic character toward a structure similar to that observed in these cosmomaterials. Both these precursors were degraded in an Ar atmosphere at 300, 500, 700 and 1000 °C over ~1 h and characterized by elemental analysis, micro-FTIR and Raman micro-spectroscopy (at 244 and 514 nm excitation wavelengths). Our results show that the precursors evolve along distinct chemical and structural pathways during carbonization and that the influence of the precursor structure is still very strong at 1000 °C. Interestingly, these different carbonization routes appear in the spectral characteristics of the G and D bands of their Raman spectra. Several of the residues present chemical and structural similarities with three recently studied ultracarbonaceous micrometeorites (Dobrica et al. [2011]. Meteorit. Planet. Sci. 46, 1363; Dartois et al. [2013]. Icarus 224, 243) and with N-rich inclusions in stratospheric IDPs. However, the residues do not simultaneously account for the carbon structure (Raman) and the chemical composition (IR, N/C ratio). This indicates that the precursors and/or heating conditions in our experiments are not fully relevant. Despite this lack of full relevancy, the formation of a polyaromatic structure fairly similar to that of UCAMMs and IDPs suggests that the origin of N-rich refractory organics lies in a thermal process in the proto-solar disk, however radiolysis cannot be excluded.

Crown Copyright © 2014 Published by Elsevier Inc. All rights reserved.

### 1. Introduction

Refractory organics (referred to as Insoluble Organic Matter in meteorites) are ubiquitous in primitive chondrites and interplanetary dust of asteroidal or cometary origin. Their abundance varies from a few wt% in chondrites up to several tens of wt% in interplanetary dust (Thomas et al., 1993). They are mostly

\* Corresponding author at: Univ. Grenoble Alpes, IPAG, F-38000 Grenoble, France.

E-mail address: [eric.quirico@obs.ujf-grenoble.fr](mailto:eric.quirico@obs.ujf-grenoble.fr) (E. Quirico).

<sup>1</sup> New addresses: Université Versailles St-Quentin, Sorbonne Universités, UPMC Univ. Paris 06, France and CNRS/INSU, LATMOS-IPSL, Guyancourt F-78280, France.

composed of carbon, hydrogen and oxygen and generally contain nitrogen and sulfur as minor elements (Alexander et al., 2007). The low nitrogen abundance with respect to the solar value deeply questions the role of nitrogen in the chemical routes that led to the formation of asteroidal and cometary organics and of the nature of the main nitrogen reservoir or reservoirs in the solar nebula and local interstellar medium (Aleon, 2010; Hily-Blant et al., 2013).

Nevertheless, rare nitrogen-rich refractory organics unrepresentative of the bulk composition have been observed in stratospheric Interplanetary Dust Particles (IDPs) (Aleon et al., 2003). They appear as tiny ( $\sim\mu\text{m}$  across) N-rich inclusions embedded in a dominant N-poor polyaromatic carbonaceous solid. Their nitrogen abundance can be as high as 20 wt%. The cyanide chemical group has been identified in one particle and their polyaromatic structure was found to be fairly – but not strictly – similar to that of IOM extracted from chondrites (Aleon et al., 2003; Dobrica et al., 2011). N-rich organics also represent the bulk of some ultracarbonaceous Antarctic micrometeorites (UCAMMs) (Dartois et al., 2013). Large N-rich inclusions of a few tens of  $\mu\text{m}$  in UCAMMs have made it possible to use a combination of spectroscopic and spectrometric techniques including secondary ion mass spectrometry (Yabuta et al., 2012; Dartois et al., 2013). These studies identified an organic solid with a polyaromatic structure somewhat similar to that of IOM from primitive chondrites, containing amine and cyanide chemical groups but small amounts of aliphatic  $\text{CH}_2$  and  $\text{CH}_3$  groups. The formation process of refractory organics in general, and in particular those N-rich inclusions, is still an enigma. Several scenarios have been proposed in the literature but none of them satisfy the all existing constraints (Kerridge, 1999; Remusat et al., 2006; Cody et al., 2011; Dartois et al., 2013; Quirico et al., 2014). Moreover, constraints may still be lacking to distinguish between different issues. For instance, the place where isotopic fractionation occurred as cold chemistry in dense cores might be very similar to the mid-plane outer regions of protoplanetary disks (Henning and Semenov, 2013).

We present here an experimental study in which analogs of N-rich refractory organics were synthesized from the thermal degradation of N-rich precursors. The general objective of these simulations was to test the possibility of a two-step process in the formation of refractory organics: synthesis of precursors under cold temperature conditions (satisfying the isotopic enrichment) and subsequent carbonization (satisfying the polyaromatic structure) (Dartois et al., 2013; Quirico et al., 2014). Two precursors were used: an HCN polymer and a *tholin* (polymeric hydrogenated carbon nitride, see for instance Quirico et al. (2008)) produced from an  $\text{N}_2:\text{CH}_4$  gaseous mixture (referred to as PHCN and tholin, respectively). They were selected for different reasons. HCN polymers have been proposed as a component of N-rich refractory organics, based on the analysis of stratospheric IDPs and interpretation of cometary distributed sources (Aleon et al., 2001; Fray et al., 2004; Cottin and Fray, 2008). These compounds form a broad family, covering a wide range of compositions and probably different degrees of polymerization. As reproducibility is a critical issue with HCN polymer, we also used a tholin produced in a cold plasma under more reproducible conditions. Using different precursors also makes it possible to investigate the so-called precursor sensitivity, i.e. the fact that the composition and structure of the final residue depend on the initial precursor. Thermal degradation was employed to produce analogs because this process is known to generate a polyaromatic structure fairly similar to that observed in chondrites, IDPs and UCAMMs (Quirico et al., 2014). As discussed below, this does not mean that a pure thermal process was at play in the astrophysical conditions. The advantage of this process is however that it can be used to produce large amounts of samples. This will provide the opportunity for reflectance

spectro-photo-goniometric measurements for the general purpose of interpreting Visible-Near InfraRed observational data of small bodies of the outer Solar System.

## 2. Materials and methods

### 2.1. Samples

Tholin samples were produced in the PAMPRE experimental reactor located at LATMOS (Guyancourt, France) (Szopa et al., 2006; Carrasco et al., 2009). PAMPRE generates a capacitively coupled plasma (CCP), confined within a cylindrical cage where molecules of the initial gaseous mixture are partially ionized and dissociated (Alves et al., 2012). Spherical tholin particles form within the plasma and are maintained under electrostatic levitation. They grow until they are big enough to fall under gravity and are collected in a glass vessel. The reactor was continuously filled with an  $\text{N}_2:\text{CH}_4 = 90:10$  gas mixture (continuous flow rate of 55 sccm) under a total pressure of 90 Pa. The power delivered by the generator of the 13.56 MHz discharge was 30 W. Several experiments were run until  $\sim 100$  mg of tholin particles were produced (typically 50 h). The samples were recovered in the form of a yellow powder, composed of spherical particles with a Gaussian size distribution: mean diameter 595 nm and standard deviation 390 nm (Hadamcik et al., 2009). This sample was basically similar to the so-called SA90 sample reported in Quirico et al. (2008) produced by PAMPRE under similar experimental conditions, and will be referred to as THO in this manuscript. THO can be described as a polymeric hydrogenated carbon nitride with  $\sim 30$  wt% soluble in methanol (Carrasco et al., 2009). Its chemical structure has not yet been fully elucidated but several functional groups have been unambiguously identified as alkyls, cyanides, amines and imines (Quirico et al., 2008; Derenne et al., 2012).

HCN polymer was produced at LISA (Université Paris-Est, Créteil) by polymerization of HCN molecules mixed with 10% ammonia, following the procedure defined by Matthews and Moser (1967). HCN was produced by reaction between NaCN (Aldrich 98%) and stearic acid  $\text{CH}_3(\text{CH}_2)_{16}\text{COOH}$  (Merck 97%). Both compounds were introduced in equimolar proportions in a vacuum manifold maintained at low pressure ( $<10^{-5}$  mbar) for a few hours in order to remove air and adsorbed water. The mixture was heated to 350 K in a dynamic vacuum to melt the stearic acid and drive its reaction with NaCN. All gases produced by the reaction (HCN, along with low quantities of formic acid and  $\text{CO}_2$ ) were condensed in a cold trap cooled with liquid nitrogen (77 K). The ice was slowly heated to 140 K to sublimate trace impurities. HCN gas purity was monitored by infrared spectroscopy. HCN and  $\text{NH}_3$  (Air Liquide 99.995%) were mixed with an  $\text{HCN}:\text{NH}_3 = 10:1$  ratio in a sealed flask maintained in a water bath to prevent any heating. The formation of HCN polymers is a slow process. In this study,  $\text{NH}_3$  was used to catalyze polymerization that lasted 51 days. They first appear as a yellow solid in the flask, which progressively turns to orange, brown and finally black. The final HCN polymer was collected after pumping of surrounding gases and was stored in an inert atmosphere to prevent oxidation. The polymerization process is however not strictly reproducible and chemical variations were observed from one sample to another. In this study, we worked with one sample, referred to as PHCN below, which is fully soluble in  $\text{CH}_3\text{OH}$  and devoid of oxygen ( $\text{H/C} = 1.19 \pm 0.02$ ,  $\text{N/C} = 1.04 \pm 0.02$ ). The PHCN infrared spectrum is displayed and compared to that of tholin in Figs. 1 and 2. We observe that PHCN contains functional groups similar to those of amines and cyanides but alkyls are not clearly detected. The narrowness of the bands basically suggests that it is chemically simpler than tholin. In particular, the very narrow cyanide band ( $\sim 2220 \text{ cm}^{-1}$ ) with almost

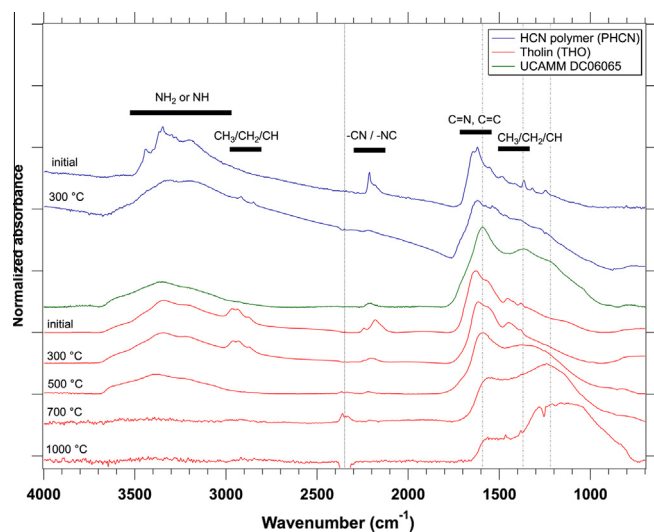


**Fig. 1.** Infrared spectra of initial PHCN and PHCN heated to 300 °C, initial THO and THO heated to 300, 500, 700 and 1000 °C and ultracarbonaceous micrometeorite DC060595 (Dartois et al., 2013). The spectrum of THO heated to 500 °C fits those of micrometeorites fairly well. Note the sequence of the chemical evolution for THO, including the subsequent loss of cyanides, alkyls and amines. The band peaking at  $\sim 1630\text{ cm}^{-1}$  in the initial THO shifts toward  $\sim 1590\text{ cm}^{-1}$  at 500 °C, consistent with the disappearance of imine groups (C=N) and emergence/increase of polyaromatic groups. A low H/C ratio at and above 700 °C is inferred from these infrared data as no hydrogen bearing terminating groups are detected. The dotted line points to the contribution of atmospheric gaseous  $\text{CO}_2$ . The dash-dotted lines indicate the positions of peaks in the spectrum of DC060595. Note that some narrow bands in the spectrum of PHCN remain unidentified.

no structure differs greatly from what is observed in tholins (Imanaka et al., 2004; Quirico et al., 2008; Vuitton et al., 2010).

## 2.2. Experimental techniques

### 2.2.1. Furnace and heating cell

Heating experiments were conducted with an ETR tubular furnace at Laboratoire des Génie des Procédés et Matériaux (Ecole Centrale Paris, France). This furnace operated in an Ar inert atmosphere up to 1200 °C. Ceramic crucibles were filled with powdered samples (5–15 mg) and carefully located in the middle of the tube to ensure a homogeneous temperature across the sample. The argon flow rate was  $30\text{ L min}^{-1}$  and the pressure within the tube was 2 bar. A  $10\text{ °C min}^{-1}$  heating rate was applied until the desired temperature was attained. The temperature was then maintained for 1 h. Finally, the furnace was allowed to cool down freely. The cooling time depended on the temperature setting and was as long as 8–9 h at 1000 °C. No *in situ* measurements could be performed within this furnace.

### 2.2.2. Elemental analysis

Bulk N/C and H/C compositions were measured on samples loaded into silver capsules (typical mass  $\sim 2\text{ mg}$ ) using a CE Instruments NC 2500 series elemental analyzer linked to a gas chromatographic column. Within the elemental analyzer, samples were combusted with ultra pure  $\text{O}_2$  at  $\sim 1000\text{ °C}$  and transformed into  $\text{CO}_2$ ,  $\text{H}_2\text{O}$  and  $\text{NO}_x$ . The resulting gases were then carried by a He flow through a column filled with Cu powder, where  $\text{NO}_x$  was reduced to  $\text{N}_2$  and excess  $\text{O}_2$  was eliminated. The final gases were then analyzed with a dedicated chromatographic column maintained under isothermal conditions and equipped with a TDC detector. The instrument was calibrated with sulfanilamide ( $\text{C}_6\text{H}_8\text{N}_2\text{O}_2\text{S}$ ).

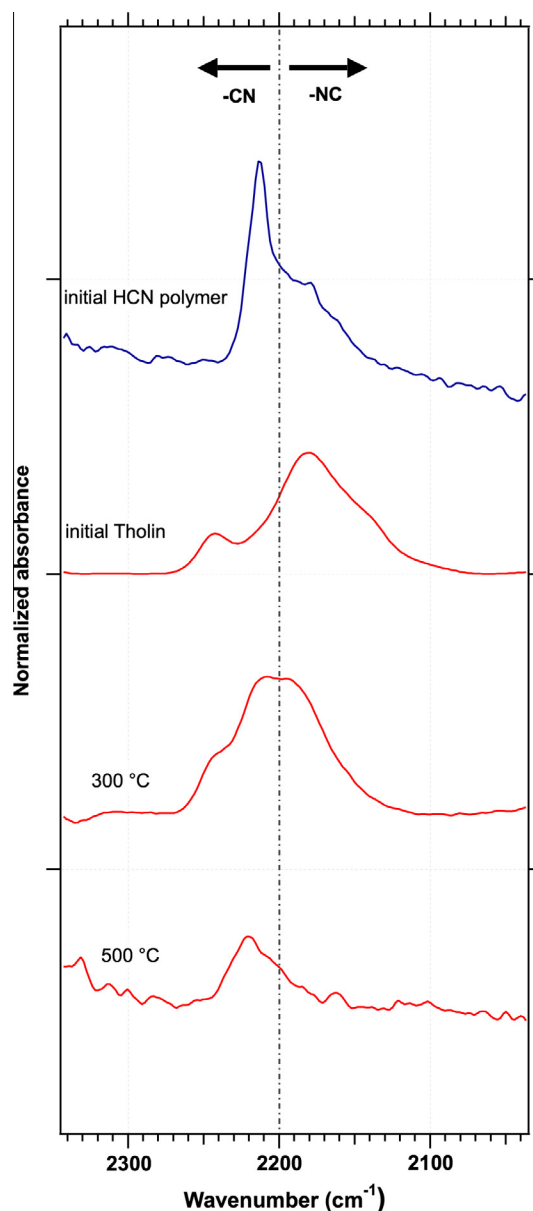


**Fig. 2.** Zoom on the  $2200\text{ cm}^{-1}$  band. Upon heating, the barycenter of the band shifts toward higher wavenumbers. This results from the structural reorganization and the possible disappearance of the isonitrile chemical groups.

### 2.2.3. Infrared and Raman spectroscopy

Infrared spectra were acquired using a Bruker Hyperion 3000 microscope linked to a Bruker Vertex FTIR spectrometer equipped with an  $\text{N}_2$  cooled MCT detector. Transmission measurements were performed in the  $700\text{--}4000\text{ cm}^{-1}$  range with a  $4\text{ cm}^{-1}$  spectral resolution. All measurements were performed in an environmental cell maintained in a secondary vacuum ( $\sim 10^{-7}\text{ mbar}$ ) that made it possible to gently heat the sample (typically  $\sim 80\text{ °C}$ ) in order to remove adsorbed water. A small amount of THO or PHCN powder ( $< 1\text{ }\mu\text{g}$ ) was deposited on a Ila diamond window (3 mm diameter, 500  $\mu\text{m}$  thick) and crushed with a similar window in order to obtain a thin, flat sample (thickness  $\sim 1\text{ }\mu\text{m}$ ).

Raman spectra were collected with 514 and 244 nm excitation wavelengths. 514 nm Raman spectra were obtained with a LabRam HR 800 (Horiba Jobin-Yvon) coupled with a Spectra Physics argon ion laser. The laser beam was focused with a  $50\times$  long-distance objective, leading to a spot diameter of 2–3  $\mu\text{m}$ . The power at the sample surface was  $300\text{ }\mu\text{W}$  and the acquisition time was 60 s.

The spectrometer was equipped with a 600 gr/mm grating and spectra were collected by a single run in the spectral range 700–2000  $\text{cm}^{-1}$ . UV Raman spectra were excited by the 244 nm wavelength of a frequency doubled argon-ion laser (Spectra Physics) and collected with a LabRam HR800 (Horiba Jobin-Yvon) designed for UV radiation. An OFR X40 objective lens was used providing a spot size of 4–5  $\mu\text{m}$ . The laser power on the surface was 100–300  $\mu\text{W}$  and the measurement duration was 6 min.

### 2.3. Analytical treatment of Raman spectra

Analytical treatment is the cornerstone of a reliable analysis of Raman spectra of disordered carbonaceous materials. The 514 nm Raman spectra of most type 1 and 2 chondrites consist of broad first-order carbon bands (the so-called G and D bands or peaks) superimposed on a fluorescence background of variable intensity (Figs. 3 and 4). A multi-step analytical procedure was applied. The first step is the extraction of the Raman bands by subtracting the fluorescence background, assuming a linear shape within the 800–2000  $\text{cm}^{-1}$  range. The peak intensity of the G band was set to 1 in order to normalize the whole data set. The second step is the extraction of the spectral information contained in the first-order carbon bands. For this purpose, we applied a so-called LBWF fit to reduced spectra, which consists in fitting the G band with a Breit–Wigner–Fano profile and the D band with a Lorentzian profile (Ferrari and Robertson, 2000). Finally, Raman spectral parameters such as width at half maximum (FWHM-G, FWHM-D), peak position ( $\omega_G$ ,  $\omega_D$ ) and ratio of peak intensity ( $I_D/I_G$ ) of the G and D bands were obtained.

The Raman spectra obtained with a 244 nm excitation exhibit no fluorescence background (Figs. 5 and 6). They were reduced using the same procedure applied to 514 nm spectra and fitted with an LBWF model. Thanks to data measured with two different excitation wavelengths, we were able to calculate the dispersion of the G-band peak position (Ferrari and Robertson, 2001).

## 3. Results

THO and PHCN as precursors were both exposed to similar thermal conditions. They were heated to 300, 500, 700 and 1000  $^{\circ}\text{C}$ , maintained at these values for 1 h and then the furnace was allowed to cool down freely (from 200 to  $\sim$ 500 min at 300  $^{\circ}\text{C}$

and 1000  $^{\circ}\text{C}$ , respectively). During heating, the samples experienced a carbonization process that led to the preferential expulsion of heteroatoms (N, H) and thus to a mass loss. For THO, the mass loss was  $\sim$ 35% at 300  $^{\circ}\text{C}$ , and 90% at 1000  $^{\circ}\text{C}$ . In the following, the THO samples heated to 300, 500, 700 and 1000  $^{\circ}\text{C}$  are designated THO300, THO500, THO700 and THO1000, respectively.

### 3.1. Tholin (THO)

Elemental compositions of THO300 and THO500 are displayed in Fig. 7. The composition of the initial tholin is very similar to that measured by Quirico et al. (2008). As the IR spectra of the SA90 and THO samples are also very similar (see below), we infer good reproducibility for the PAMPRE production process. Upon heating, the H/C and N/C elemental ratio both decrease, consistent with a carbonization process that tends to concentrate elemental carbon in the residue. No elemental composition could be determined above 500  $^{\circ}\text{C}$ , due to the low mass of the residues. However, we can reasonably infer that both these ratio will continue to decrease upon further heating up to 1000  $^{\circ}\text{C}$ .

The IR spectrum of the initial THO has been addressed in detail by several publications (Mutsukura and Akita, 1999; Imanaka et al., 2004; Quirico et al., 2008). The main chemical groups that have been identified are: primary and/or secondary amine groups, methyl ( $\text{CH}_3$ ) and methylene ( $\text{CH}_2$ ) groups, cyanides  $-\text{CN}$  (possibly isocyanides  $-\text{NC}$ ) and imines  $\text{C}=\text{N}$  (Fig. 1). Upon heating, we observe that the cyanide abundance dramatically decreases between ambient temperature and 300  $^{\circ}\text{C}$ , is hardly detectable at 500  $^{\circ}\text{C}$  and undetected above. The shape of the band at  $\sim$ 2200  $\text{cm}^{-1}$  also evolves upon heating: its peak position (for the feature with highest intensity in the case of initial THO) shifts toward high wavenumbers from ambient temperature up to 500  $^{\circ}\text{C}$  and the width of the band decreases between room temperature and 500  $^{\circ}\text{C}$  (Fig. 2). The alkyl chemical groups are detected in similar abundances up to 300  $^{\circ}\text{C}$  and disappear between 300 and 500  $^{\circ}\text{C}$ . Primary and secondary amine functional groups are more resistant to thermal heating and are still present in significant abundance at 500  $^{\circ}\text{C}$ . They disappear between 500 and 700  $^{\circ}\text{C}$ . At 700  $^{\circ}\text{C}$  and above, the contribution of hydrogenated bonds is weak or negligible, suggesting that the hydrogen to carbon ratio (H/C) decreased dramatically above 500  $^{\circ}\text{C}$  and was finally much lower than 0.2. Below 1700  $\text{cm}^{-1}$ , the IR spectra consist of a broad feature

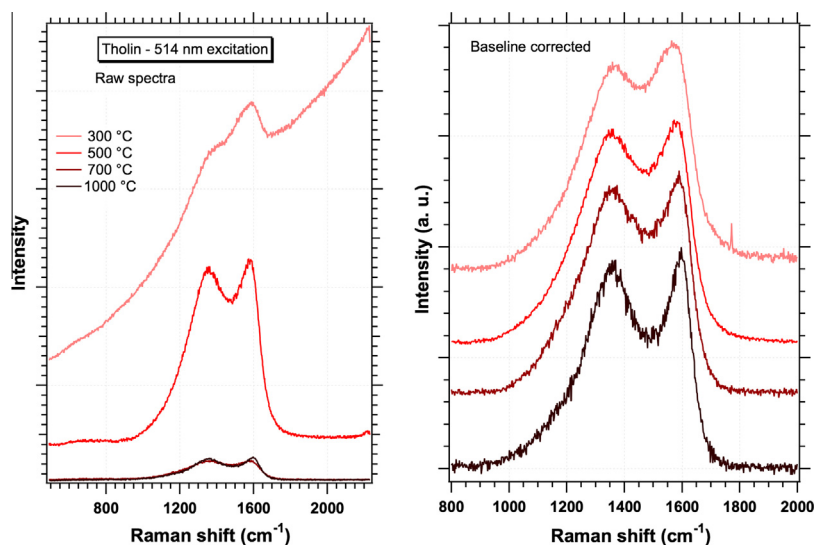
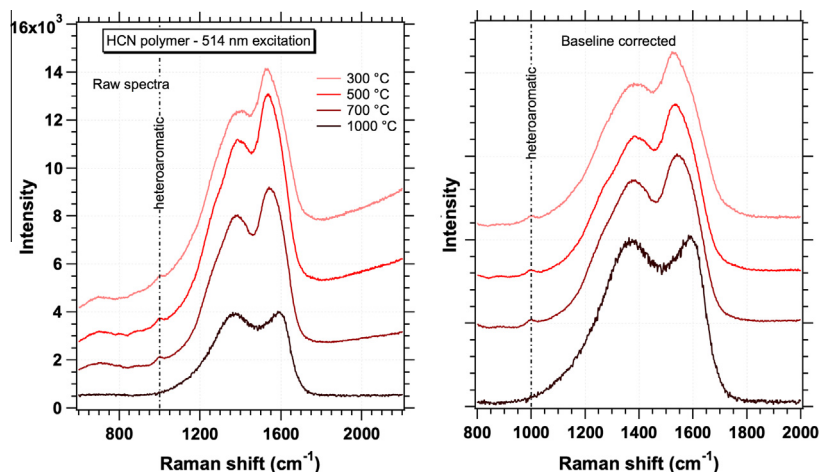
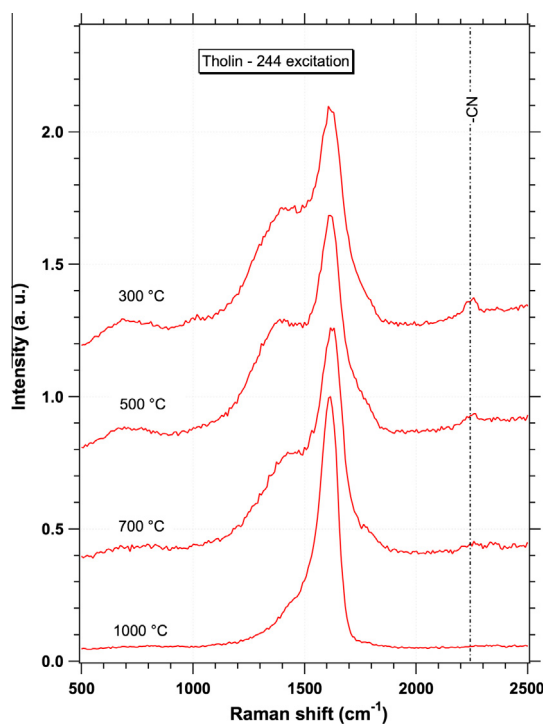


Fig. 3. Raman spectra of heated THO acquired with a 514 nm excitation. Left: raw spectra. Right: reduced spectra after baseline correction and normalization to 1 of the G band intensity. The fluorescence is very high in the spectrum of THO heated to 300  $^{\circ}\text{C}$ . The first-order carbon bands are observed for all samples.



**Fig. 4.** Raman spectra of PHCN heated to 300, 500, 700 and 1000 °C acquired with a 514 nm excitation. Left: raw spectra. Right: reduced spectra after baseline correction and normalization of the G band. The general shape of the G and D bands is different than those in THO spectra, indicating a precursor effect. The mixed line points to a weak and narrow feature that can be assigned to small heteroaromatic groups. Its disappearance at 1000 °C is triggered by aromatic condensation. Note the very specific shape of the bands with respect to THO residues (see Fig. 3).



**Fig. 5.** Raman spectra of heated THO samples recorded with a 244 nm excitation. The main trend observed is a decrease in the intensity of the D band. The dash-dotted line shows the weak feature assigned to the nitrile chemical group.

with two peaks at 1558 and 1242  $\text{cm}^{-1}$  (700 °C), a plateau between 1570 and 1400  $\text{cm}^{-1}$  and a broad band peaking at 1170  $\text{cm}^{-1}$  (1000 °C). This broad feature results from the contributions of a large variety of chemical groups. Some of them exist only in the solid state. Hence, nitrogen can be considered as a dopant in amorphous carbon solids. In this respect, trivalent nitrogen bonded to adjacent carbon atoms (tertiary amines) and tetrahedral N+ sites compensated by charges in the gap have been proposed on the basis of X-ray Absorption Near Edge Structure at the nitrogen K-edge spectra (Robertson and Davis, 1995).  $\text{Sp}^2$  bonded nitrogen is also present as pyrrole or pyridine-like fivefold and sixfold rings, respectively. A nitrogen dopant in a pyridine-like unit has a tetrahedral configuration and has also been proposed as a component of

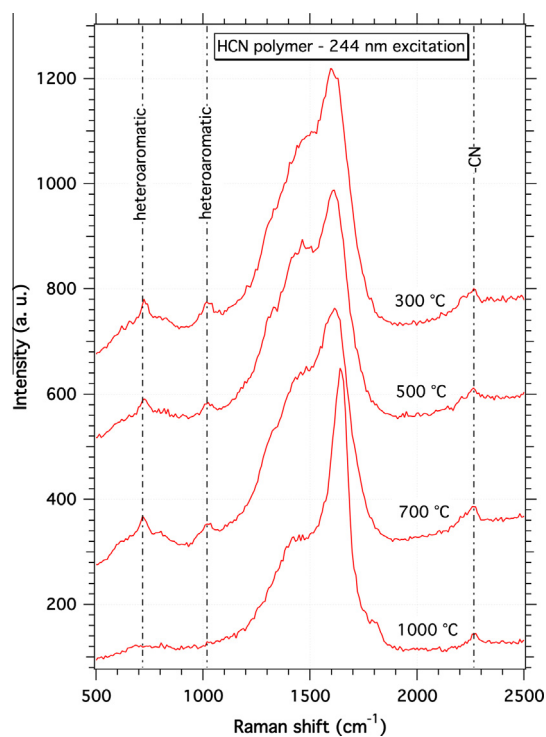


**Fig. 6.** Raman spectra of heated PHCN samples recorded with a 244 nm excitation. The main trend observed is a decrease in the intensity of the D band. Note that at 1000 °C, the intensity of the D band remains much higher than for THO, indicating that the latter reached a more advanced stage in carbonization. The dash-dotted lines indicate weak and narrow features that can be assigned to small heteroaromatic groups (at  $\sim 710$ , 1000  $\text{cm}^{-1}$ ) and nitriles and/or isonitriles (at  $\sim 2270$   $\text{cm}^{-1}$ ). The disappearance of the features due to heteroaromatics at 1000 °C is triggered by aromatic condensation.

N-rich carbon nitrides. Finally, due to spectral congestion and solid state effects, it is not possible to identify specific groups and to derive quantitative information. However, we point out that the main peak at  $\sim 1630$   $\text{cm}^{-1}$ , mostly due to imine groups, shifts to  $\sim 1590$   $\text{cm}^{-1}$  at 500 °C (Fig. 1). This shift is due to the appearance and the increasing abundance of polyaromatic units upon heating.

Our results agree qualitatively with those of Mutsukura and Akita (1999). In their study, an initial sample fairly similar to

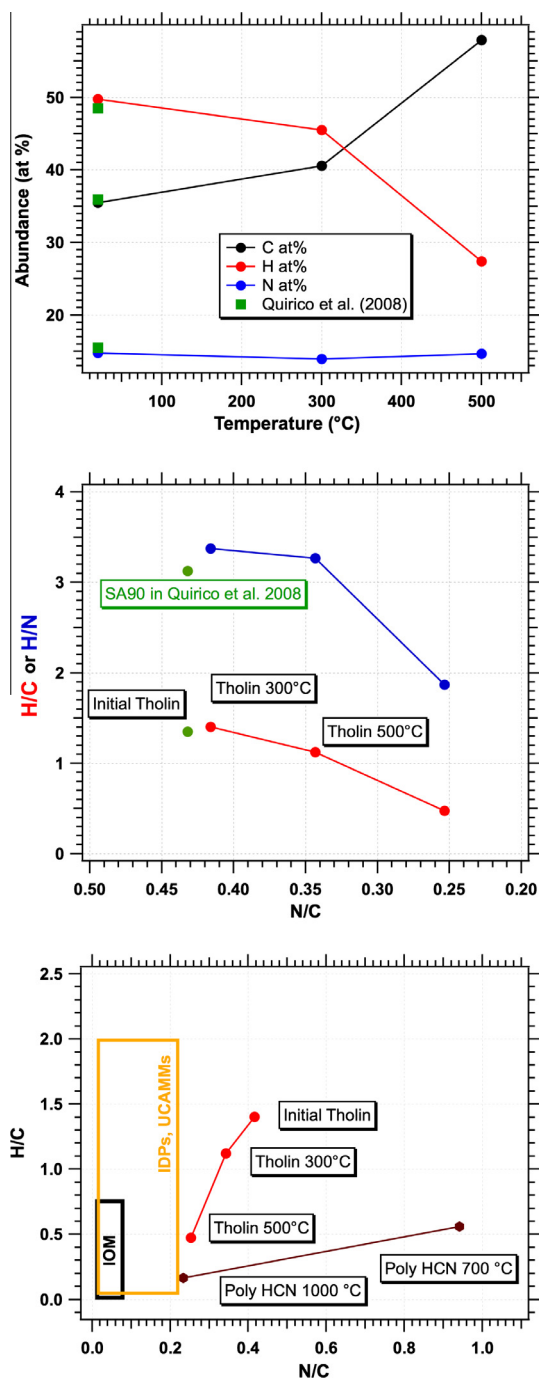


**Fig. 7.** Top: atomic abundance of C, H and N elements of initial THO and THO heated to 300 and 500 °C (no measurements could be made at 700 and 1000 °C). Middle: H/C vs. N/C ratio for initial THO and PHCN heated to 300 and 500 °C. Both these ratios are expected to decrease upon heating up to 1000 °C. Bottom: H/C vs. N/C ratio plotted for initial and heated THO and PHCN and comparison with cosmomaterials. Orange and black rectangles represent the variations of values reported in the literature for IDPs and UCAMMs and for chondritic IOM, respectively (Dartois et al., 2013; Aleon et al., 2001, 2003). (For interpretation of the references to colour in this figure legend, the reader is referred to the web version of this article.)

THO was annealed and IR spectra were recorded up to 500 °C. The different chemical groups were expelled in the same order as in our study: cyanides, alkyls and amines. However, there were two differences. First, the chemical groups were expelled at lower temperatures. For instance, at 500 °C, the infrared spectrum was almost devoid of amine groups while this was far from the case

in our data. Second, the broad feature they observed between 1600 and 800  $\text{cm}^{-1}$  was basically different than what we observe. In particular it contained substructures. These differences can be due to different starting materials, different heating conditions or possibly a different time–temperature history.

We performed Raman measurements at two excitation wavelengths: 514 nm and 244 nm. At 514 nm, the initial tholin was extremely fluorescent and no spectra could be collected. At 300 °C, the fluorescence background still had a high intensity but first-order carbon bands were detected. At 500 °C and above, the fluorescence background was negligible and Raman spectra of good quality could be measured (Fig. 3). The Raman spectral parameters of the samples are plotted in Fig. 8 and listed in Table 1. THO500 and THO700 have a high FWHM-D ( $\sim 290 \text{ cm}^{-1}$ ), with  $I_D/I_G$  ranging between 1 and 1.2. At 1000 °C, FWHM-D is much lower ( $\sim 245 \text{ cm}^{-1}$ ). The data for THO300 are scattered and likely reflect

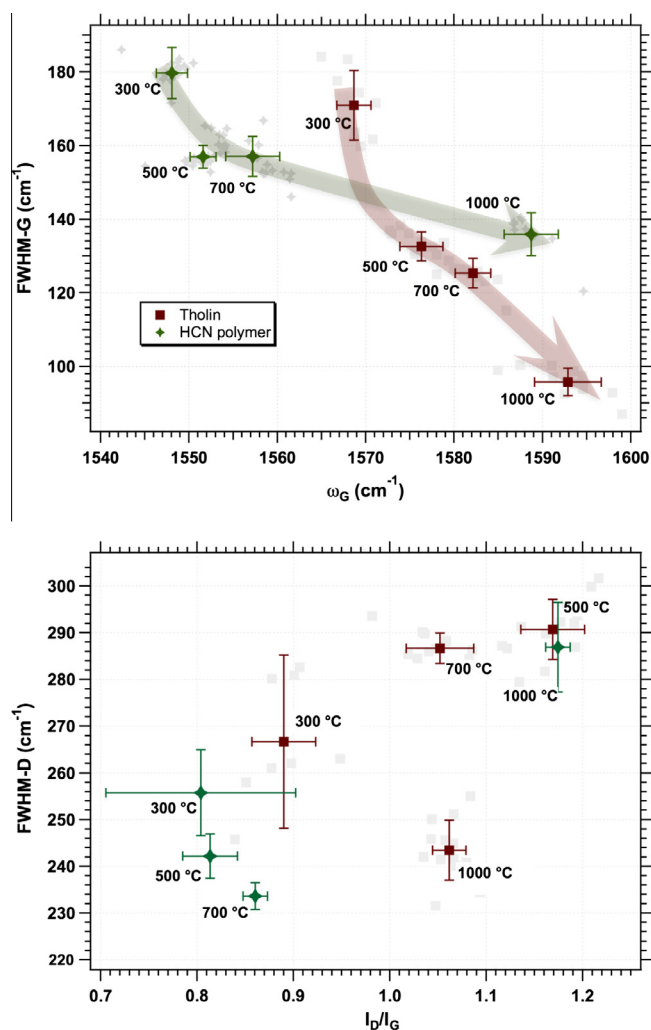


**Fig. 8.** The Raman spectral parameters extracted from the 514 nm Raman spectra using a Lorentzian–Breit–Wigner–Fano fit model. Top: width of the G band plotted against its peak position. In this diagram both THO and PHCN display a trend characterized by the decrease of FWHM-G and increase of  $\omega_G$ . Note that these trends are distinct, reflecting different polyaromatic structures during the carbonization process (the so-called precursor effect). Under similar heating conditions, THO is more extensively carbonized than PHCN. Bottom: width of the D band plotted against the ratio of peak intensity. For all samples, the width of the D band is high and provides almost no information on the structure. The degree of structural order of the samples remains very low. Faint gray points are parameters from individual spectra. Note that the Raman spectra of the starting THO and PHCN could not be measured due to the high fluorescence background.

**Table 1**  
514 nm Raman parameters.

	FWHM-G (cm <sup>-1</sup> )	$\omega_G$ (cm <sup>-1</sup> )	$I_D/I_G$	FWHM-D (cm <sup>-1</sup> )	$\omega_D$ (cm <sup>-1</sup> )
THO300	171 ± 10	1568.6 ± 1.9	0.89 ± 0.04	267 ± 19	1360.4 ± 1.9
THO500	132.6 ± 4.0	1576.3 ± 2.4	1.05 ± 0.04	287 ± 4	1354.7 ± 2.4
THO700	125.4 ± 3.7	1582.1 ± 3.8	1.17 ± 0.02	291 ± 7	1352.9 ± 3.7
THO1000	95.8 ± 3.7	1592.7 ± 3.8	1.06 ± 0.02	243 ± 7	1352.0 ± 2.8
PHCN300	179.8 ± 7.0	1548.1 ± 1.8	0.80 ± 0.10	255.7 ± 9.2	1375.8 ± 7.5
PHCN500	157.0 ± 3.1	1551.6 ± 1.5	0.81 ± 0.03	242.3 ± 4.8	1360.2 ± 1.5
PHCN700	157.0 ± 5.4	1557.3 ± 3.0	0.86 ± 0.02	233.7 ± 2.9	1355.5 ± 3.0
PHCN1000	135.9 ± 5.8	1588.7 ± 3.0	1.17 ± 0.02	286.9 ± 9.6	1371.0 ± 2.9

strong perturbations of the broad D band by the fluorescence background. The narrower G band is less blurred by fluorescence and its spectral parameters are more reliable. On a FWHM-G vs.  $\omega_G$  diagram, we observe a gradual decrease of FWHM-G along with increasing  $\omega_G$ .

UV 244 nm Raman spectra are devoid of fluorescence and exhibit an intense and narrow G band and a weaker D band that appears as a shoulder toward low wavenumbers (Fig. 5). The most dramatic spectral change observed upon heating is the strong decrease of the D band intensity between 700 and 1000 °C, which could be explained by ring condensation and the extent of polyaromatic units. We also observe that FWHM-G and  $I_D/I_G$  continuously decrease upon heating, suggesting a continuous polyaromatic reorganization. UV Raman spectra also display resonant features. Cyanide is detected up to 500 °C by the feature peaking at ~2200 cm<sup>-1</sup> and is undetected above, consistent with IR measurements.

The dispersion of the peak position of the G band is the ratio of the range of variation of  $\omega_G$  over the range of variation of the excitation wavelength. This parameter is of primary importance to characterize the sp<sup>2</sup> structure of carbon materials, providing less ambiguous information than data acquired with a single wavelength excitation (Ferrari et al., 2003). We could calculate this parameter thanks to our data measured at 514 and 244 nm. It evolves from 0.25 cm<sup>-1</sup>/nm down to 0.10 cm<sup>-1</sup>/nm, consistent with the settling of a polyaromatic structure (Ferrari et al., 2003).

### 3.2. HCN polymer (PHCN)

The elemental composition of PHCN residues could be measured only for 700 and 1000 °C due to the small amount of material that prevented a comprehensive set of measurements (Fig. 7). At 700 °C, the N/C ratio is close to the value of the starting material, while the H/C ratio lies around 0.5, compared to 1 for the initial material (Bonnet et al., 2013). At 1000 °C, the N/C ratio lies around 0.2 and H/C is ~0.15. Infrared spectra could be collected only for the initial HCN polymer and the residue obtained at 300 °C. The infrared spectrum of the initial PHCN (Fig. 1) reveals the same main functional groups as observed in tholin spectra, except for alkyl groups. However, the spectrum has a different appearance with much narrower bands due to these chemical groups superimposed on broader structures. This probably reflects the fact that the material is chemically simpler than THO. Bonnet et al. (2013) observed that it was fully soluble in methanol, therefore indicating that it does not contain an insoluble covalent solid fraction and that solid-state effects that tend to broaden the bands are weak. Upon heating to 300 °C, the appearance of the IR spectrum is more similar to that of THO as we observe broader bands, consistent with the formation of a covalent structure. The cyanide band is much lower and surprisingly faint features attributable to alkyl groups are observed. They could be related to contamination but more probably reflect a mechanism that would preferentially stabilize alkyls during the first stages of the carbonization process. Indeed, the alkyl bands may be too faint to be detected in the

starting material but alkyls could be present. This has already been observed in tholin samples (see Fig. 4 in Carrasco et al. (2009)).

Raman measurements were performed under the same conditions as for THO residues. At 514 nm, the initial PHCN was extremely fluorescent and no spectra could be collected. Spectra collected between 300 and 1000 °C are displayed in Fig. 4 and their Raman spectral parameters extracted with the Lorentzian–Breit–Wigner–Fano method in Fig. 8 and Table 1. They show G and D bands similar to those observed for THO, as well as a faint feature at ~1000 cm<sup>-1</sup> that is due to heteroaromatic units. This feature disappears at 1000 °C due to the condensation of these units. As observed for residues from THO, FWHM-D remains large even at 1000 °C, showing that the more carbonized residue is structurally very disordered. The width of G band remains higher than for THO1000, showing that PHCN attained a lower degree of structural order than THO under similar heating conditions. These observations are confirmed by 244 nm Raman measurements (Figs. 6 and 9). Two faint features at ~700 and 1000 cm<sup>-1</sup> are observed and are assigned to heteroaromatic compounds. As observed in 514 nm Raman spectra, these features disappear at 1000 °C due to ring condensation. At 1000 °C, the intensity of the D band is higher than in the spectrum of THO1000, confirming that PHCN attained a lower degree of structural order.

## 4. Discussion

### 4.1. Thermal degradation process

The evolution of PHCN and THO as precursors is controlled by a combination of several mechanisms: (1) sublimation of low weight

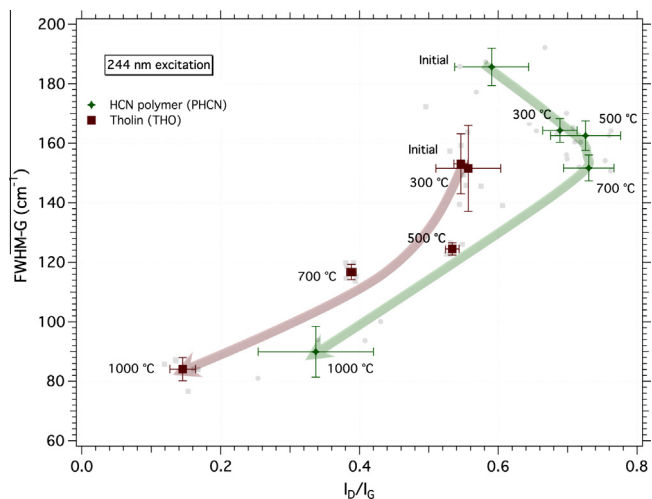


**Fig. 9.** The width of the G band plotted against  $I_D/I_G$ , determined from 244 nm Raman spectra. Both heated THO and PHCN display distinct evolution trends. Faint gray points are parameters from individual spectra.

molecules, (2) bond breaking and expulsion of chemical groups and (3) bond creation and cross-linking. This constitutes the so-called *carbonization* process that leads to mass loss, increase of carbon concentration and continuous reorganization of the chemical structure. Nna-Mvombo et al. (2013) studied the thermal degradation of tholin samples using thermogravimetry/mass spectrometry, differential thermal analysis and differential scanning calorimetry. They identified three main sequences: (1) moisture disappearance (<150 °C), (2) a pyrolysis stage between 150 and 575 °C, consisting in dominant endothermic reactions expelling various chemical groups, and (3) a “carbonization” stage above 575 °C. In their study they use the term carbonization to describe the sequence above 575 °C characterized by a significantly lower mass loss than in the second stage. In our study, the so-called carbonization stage covers the whole thermal degradation process above 150 °C, consistent with the terminology widely used in organic geochemistry. In their experiment, the temperature of 575 °C was reached with a continuous heating rate of 10 °C/min, i.e. lasting for a duration of ~1 h. For their sample termed tholin 2, very similar to THO heated to 1000 °C, the reflectance infrared spectrum shows two prominent features at 1364 and 1397 cm<sup>-1</sup> and the absence of bands due to alkyls, amines and nitriles. This is fairly similar to the infrared spectrum of THO700. We thus reasonably infer that THO heated above 700 °C expels much lower amounts of chemical groups.

As soon as carbonization begins, the solid starts aromatizing and a polyaromatic structure forms, consisting of polyaromatic units bridged to each other through various functional groups (Vandenbroucke and Largeau, 2007). A polyaromatic structure emerges in both precursors at 300 °C. Hence, the Raman spectra display well separated G and D bands for a 514 nm excitation, a narrow G band and a weak intensity of the D band for 244 nm excitation, typical of polyaromatic solids like chondritic IOM or terrestrial kerogens. The  $\omega_C$  dispersion is however still high (0.25 cm<sup>-1</sup>/nm) compared to the dispersion observed in chondritic IOM, terrestrial kerogens or coals (Quirico et al., 2014). Therefore, at 300 °C, we observe the very first stages of the appearance of a polyaromatic structure.

The structure/composition of a heated precursor depends on several parameters such as its initial structure and composition, the presence of pressure, its time–temperature history and other factors (e.g. oxygen fugacity, presence of liquid water) (Bény-Bassez and Rouzaud, 1985; Bernard et al., 2010). Our data show that PHCN and THO exhibit different structural and chemical evolution even though similar physical conditions were applied. Bond creation and cross-linking occurred leading to the partial polymerization of the initial soluble PHCN. At 300 °C, the PHCN residue is a black solid mostly insoluble in common solvents. The soluble fraction of THO probably underwent a similar process, while the insoluble fraction started degrading. Optical and Raman microscopic survey of the residues of THO suggest a homogeneous solid and the full disappearance of the starting precursor. However, the carbonization rate of PHCN is lower than that of THO. The N/C ratio of THO500 is somewhat similar to that of PHCN heated to 1000 °C. The Raman data also show that the ordering rate of the polyaromatic structure is slower in PHCN. FWHM-G is a reliable parameter for ordering in very disordered carbonaceous materials (Busemann et al., 2007). Here we observe that the width of the G band (FWHM-G) determined from the 514 nm spectra is greater for PHCN (~135 cm<sup>-1</sup>) than for THO (90 cm<sup>-1</sup>) heated to 1000 °C. The intensity of the D band in the 244 nm spectra also points to the presence of very small polyaromatic units in PHCN, which have mostly disappeared in THO. The smaller the excitation wavelength, the smaller the sp<sup>2</sup> cluster probed by Raman spectroscopy (Ferrari and Robertson, 2001). In contrast, the D-band (FWHM-D) remains wide in the 514 nm Raman data, even at 1000 °C (>200 cm<sup>-1</sup>; Fig. 6).

Interestingly, the precursor effect between PHCN and THO appears clearly in the shape of the G and D bands (Figs. 3 and 4) and in the extracted Raman spectral parameters (Figs. 8 and 9). Precursor effects have been observed experimentally in the Raman spectra of anthracene and saccharose-based cokes (Bény-Bassez and Rouzaud, 1985; Rouzaud and Oberlin, 1990; Bernard et al., 2010) and have been suspected in natural kerogens (Quirico et al., 2009). These experimental studies used precursors that had been previously carbonized (saccharose and anthracene crystals) and the precursor effect is less obvious at 1000 °C than in our data (see Fig. 2 in Bernard et al. (2010)). It is plausible that the explanation for the stronger precursor effect lies in the higher chemical complexity of PHCN and THO with respect to anthracene molecular crystals and saccharose. A better understanding will require systematic studies on series of precursors with increasing chemical complexity.

#### 4.2. Comparison with stratospheric IDPs and UCAMMs

In order to evaluate the relevancy of the residues produced from the tholin and PHCN samples, we compared their chemical and structural properties with those of N-rich inclusions in stratospheric interplanetary dust particles (IDPs) and ultracarbonaceous Antarctic micrometeorites (UCAMMs).

We first consider Raman data obtained with a 514 nm excitation. The residues produced by heating tholin and PHCN exhibit a polyaromatic structure that is fairly (but not exactly) similar to that observed in UCAMMs, Antarctic micrometeorites and stratospheric IDPs. In a FWHM-G vs.  $\omega_C$  diagram (Fig. 10a), residues that best fit UCAMMs are the tholin samples heated to 500, 700 and 1000 °C. They are all close to the data points of the three UCAMMs, even though they do not match them exactly. Hence, data points of DC060565 and DC060594 are only partially covered by THO500 and THO1000, respectively. A part of these discrepancies may be due to the different experimental conditions employed for the Raman measurements, but this contribution is expected to be small given that the linear FWHM-G vs.  $\omega_C$  trends measured by different operators are fairly close (Fig. 10a; Busemann et al., 2009; Dobrica et al., 2011; Quirico et al., 2014). Interestingly, we observe that for DC06-09-19;45;119, and to a lesser extent for DC060565, data values span over a much broader range of variation compared to tholin residues. This points to a higher structural heterogeneity of this UCAMM. Considering the IDP trend of Busemann et al. (2009), we also observe that residues from the tholin sample provide better fits than PHCN. In contrast, in a FWHM-D vs.  $I_D/I_G$  diagram, we observe that the  $I_D/I_G$  parameter of tholin residues is generally larger than in UCAMMs, while those of residues from PHCN are consistent with UCAMMs (Fig. 10b). The width of the D band is not a reliable parameter for such disordered carbonaceous materials. As mentioned in Section 4.1, the general shape of the G and D bands is very different for each of the two groups of residues (Figs. 3 and 4). In this respect, tholin residues appear more consistent with UCAMMs than PHCN residues. Finally, 244 nm Raman spectra of the UCAMM DC06-09-19;45;119 and IDP L2008X3 are consistent with those of most HCN polymer and tholin residues, except with the tholin heated to 1000 °C (see Fig. 6 in Dobrica et al. (2011)).

IR spectra and N/C ratios are only available for two UCAMMs: DC060565 and DC060594 (Dartois et al., 2013). The IR spectrum of DC060565 is best fitted by THO500 (Fig. 1). The amine band has a very similar shape and intensity and the intense aromatic C=C band has a position very close to that of the UCAMM (1592 cm<sup>-1</sup>). There are however differences such as a weaker –CN band, a larger and less structured C=C band at 1592 cm<sup>-1</sup> and less structure in the broad band at ~1480 cm<sup>-1</sup>, with no peaks at 1370 and ~1220 cm<sup>-1</sup>. The N/C value of THO500 lies near the

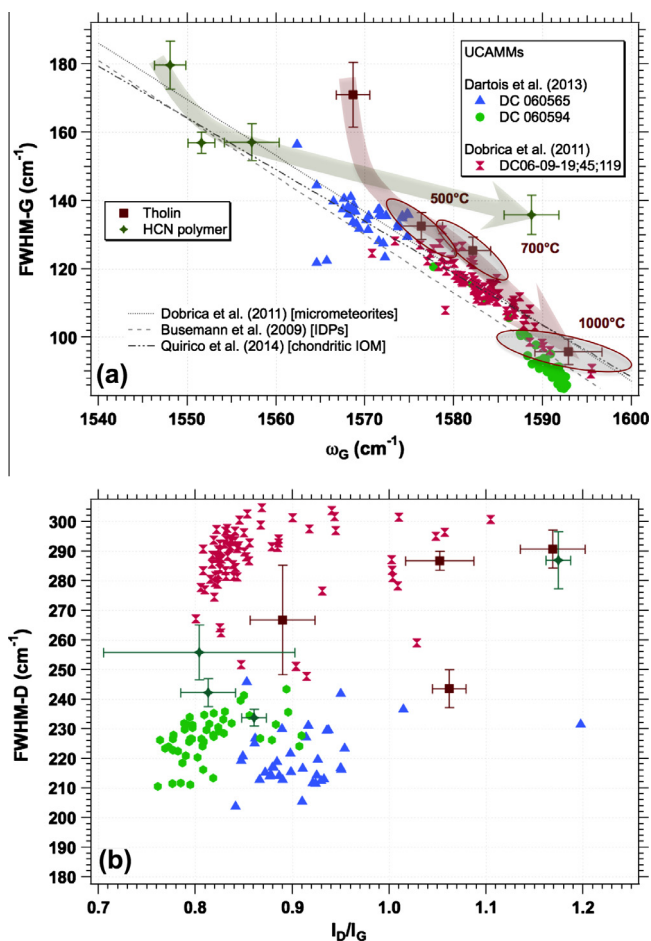


**Fig. 10.** Comparison of 514 nm Raman spectral parameters of THO and PHCN with those of the micrometeorites studied by Dartois et al. (2013) and Dobrica et al. (2011). (a) FWHM-G vs.  $\omega_G$  diagram. (b) FWHM-D vs.  $\omega_D$  diagram. The best matches are obtained for THO heated between 500 and 1000 °C. Ellipses display the range of variation of data points. The lines indicate the trend measured for IDPs (Busemann et al., 2009), AMMs (Dobrica et al., 2011) and carbonaceous chondrites (Quirico et al., 2014).

upper limit of the distribution measured by nanoSIMS (Dartois et al., 2013). As already pointed out, the Raman spectrum of THO500 does not very well match that of DC060565. A tholin heated to a lower temperature could provide a more relevant residue. But in this case the N/C ratio would be definitely too large. We observe that by combining structural and chemical information, we more accurately constrain the relevance of the analogs.

For the UCAMM DC060594, the IR spectra appear to agree fairly well with those of THO500, as already observed (except for the broad band that peaks at  $\sim 1480\text{ cm}^{-1}$ ). However, in this case, the best Raman match (with a 514 nm excitation) is obtained with THO1000, which has a very different IR spectrum. Note that the 244 nm Raman spectrum does not fit that of the UCAMM DC06-09-19;45;119, but unfortunately we do not have 244 nm Raman spectra of the UCAMMs studied by Dartois et al. (2013). There is clearly a major disagreement between structure and composition.

Regarding these observations, it is difficult to infer the relevancy of our residues for the UCAMM DC06-09-19;45;119 (Dobrica et al., 2011) and of stratospheric IDPs as no chemical information is generally available in the literature. Even the Raman data may lack the description of parameters. For instance, Busemann et al. (2009) report the FWHM-G and  $\omega_G$  parameters, but not  $I_D/I_G$ . Some studies report XANES measurements at the K-edge, but such data are not available for our residues (Flynn

et al., 2003; Busemann et al., 2009). Based on measurements of the H/C ratio in 5 stratospheric IDPs, Aleon et al. (2001) suggested that H/C varies over  $\sim 0.33\text{--}2$ . However, this parameter may be blurred by strong instrumental fractionation. The N/C ratio would appear to be a more robust parameter. In stratospheric IDPs, local values of around 10–20 wt% have been proposed in the literature for D-rich regions (Aleon et al., 2003). These values match those of the UCAMMs (from  $\sim 4$  to 17 at%) and refer to residues obtained above 500 °C.

Our results strongly suggest that characterization of stratospheric IDPs and Antarctic Micrometeorites needs to combine structural and chemical information and to fully exploit Raman information including the whole set of spectral parameters FWHM-G,  $\omega_G$ ,  $I_D/I_G$ , FWHM-D and  $\omega_D$ . The shape of the first-order carbon bands should also be taken into account and the use of at least two excitation wavelengths is required to avoid all ambiguity. Furthermore, combining imaging measurements at the micrometric scale represents a challenge given that natural samples are heterogeneous.

#### 4.3. Formation process of N-rich refractory organics

The polyaromatic structure of N-rich refractory organics suggests that these compounds were formed or have evolved through energetic processes such as *thermal heating* or *radiolysis*. Thermal heating may have occurred in the inner solar nebula. Numerical simulations of proto-planetary disks suggest a broad range of temperatures up to  $\sim 2000\text{ K}$  with durations up to several Ma (Henning and Semenov, 2013). In addition, chondrules in primitive meteorites indicate the presence of high temperature and short duration heating, possibly triggered by shock waves, lightning or other phenomena (Hewins, 1997; Krot et al., 2009). A peak temperature within the range 1500–1900 °C over <1 min duration has been estimated. These time–temperature conditions vary over several orders of magnitude and no constraint on the presumed heating conditions of UCAMMs is provided.

Cometary grains may have been heated in the interplanetary medium during their transit to Earth (Kolokolova et al., 2004; Fray et al., 2006). This is however not of concern for UCAMMs or most IDPs due to their size that is much larger than a few micrometers and their heliocentric distance. Deceleration in the atmosphere is also a possible source of heating under oxidizing conditions. Effects of atmospheric flash-heating can be detected from Raman spectra and no detectable heating effects have been reported for UCAMMs recently analyzed in the literature (Dobrica et al., 2011). According to the composition of GEMS phases, UCAMMs may not have been heated above 300 °C (Bradley et al., 2014). Given the very short duration of this heating, the consequences on composition and structure on organics are expected to be small.

Alternatively, Dartois et al. (2013) suggested that N-rich UCAMM precursors formed within the  $\text{N}_2$ -rich subsurface of comets in the Oort cloud by action of Galactic swift ion (Cosmic Rays) radiolysis. This scenario clearly identifies a nitrogen-rich medium required to form organics with high nitrogen abundance and would account for the absence of N-rich refractory organics in chondritic IOM. In this respect, an origin from the outer Solar System appears more plausible than formation in the inner solar nebula followed by turbulent transport. However, a pending issue lies in the formation of a polyaromatic solid by ion irradiation. The formation of refractory carbonaceous solids from ice mixtures has been investigated in several studies (Strazzulla et al., 2001; Palumbo et al., 2004; Baratta et al., 2008; Pilling et al., 2010). Brucato et al. (2006) formed a carbonaceous film by irradiating formamide ice, the IR spectrum of which displays broad features including amines and nitriles. Most of the studies that combined

ice irradiation and Raman characterization of the residues operated with ion beams in the keV range, implying that a significant fraction of energy is deposited through nuclear interaction. Raman characterization indicated amorphous carbonaceous residue and therefore the lack of a polyaromatic structure. There is an apparent contradiction in the sense that settling and developing a polyaromatic structure involves an increase in the structural order (Ferrari et al., 2001) while irradiation in the keV range generates disorder. For example, irradiation of soot samples leads to breaking of large polyaromatic units (Brunetto et al., 2009). However, irradiation by swift heavy ions, that trigger essentially electronic interaction, effectively carbonizes simple polymers and induces a polyaromatic structure (Costantini et al., 2002, 2005).

Finally, the fact that reasonable analogs of refractory organics are produced by thermal degradation is of interest for the production of surface analogs of Solar System bodies. Indeed, radiolysis experiments are performed on films and very small amounts of material, preventing reflectance spectro-photo-goniometric measurements (Bernard et al., 2006; Beck et al., 2012). Heating experiments can produce several hundreds of mg of samples and are available for such measurements.

## 5. Conclusion

The main conclusions are the following:

1. The carbonization of an HCN polymer and a tholin results in the preferential loss of H and N heteroatoms and is accompanied by the emergence of a polyaromatic structure. At 1000 °C, both precursors still contained a significant fraction of nitrogen, with no alkyl, nitrile or amine groups.
2. Both precursors experienced distinct chemical and structural evolution. The tholin sample carbonized more easily than PHCN under similar heating conditions and led to residues with more organized structures. Looking more closely, this precursor effect results in distinct polyaromatic structures that can be traced though the spectral characteristics of the first-order carbon bands in the Raman spectra. The precursor effect is strong.
3. Residues that best fit the Raman characteristics of the UCAMMs were produced from the tholin sample. They reasonably account for the presence of a poorly ordered polyaromatic structure in N-rich UCAMMs and N-rich inclusions in stratospheric IDPs and for the range of variation of the N/C ratio. However, taking a closer look, none of the residues accurately account for both the carbon structure (Raman) and the chemical composition (IR, N/C ratio). This result may indicate that tholin and PHCN are not relevant precursors, however kinetic effects and co-factor influences should be explored before drawing a firm conclusion.
4. To gain further insight into the nature of N-rich refractory phases such as UCAMMs or inclusions in stratospheric IDPs simultaneous collection of structural and chemical information will be required, for instance by combining imaging on the same samples at a micrometric spatial scale to take heterogeneity into account.
5. The polyaromatic structure of UCAMMs may be the result of the past action of an energetic process, which could be either thermal heating in the inner proto-solar disk or radiolysis by swift heavy ions in the outer region of the proto-solar disk or in the Oort cloud. Further investigations based upon irradiation experiments are required to decipher the respective contributions of these two processes.
6. Thermal degradation can be used to produce large amounts of analogs, opening the way to reflectance spectro-photo-goniometric measurements necessary for the interpretation of reflectance data of outer Solar System bodies.

## Acknowledgments

This work has been funded by the Centre National d'Etudes Spatiales (CNES-France) and by the ANR COSMISME project Grant ANR-2010-BLAN-0502 of the French Agence Nationale de la Recherche. The Raman facility at Ecole Normale Supérieure de Lyon is supported by the Institut National des Sciences de l'Univers (INSU). We are very grateful to Hikaru Yabuta (Osaka University) and an anonymous reviewer for very fruitful comments that greatly improved the quality of the manuscript.

## References

- Aleon, J., 2010. Multiple origins of nitrogen isotopic anomalies in meteorites and comets. *Astrophys. J.* 722, 1342–1351.
- Aleon, J., Engrand, C., Robert, F., Chaussidon, M., 2001. Clues to the origin of interplanetary dust particles from the isotopic study of their hydrogen-bearing phases. *Geochim. Cosmochim. Acta* 65, 4399–4412.
- Aleon, J., Robert, F., Chaussidon, M., Marty, B., 2003. Nitrogen isotopic composition of macromolecular organic matter in interplanetary dust particles. *Cosmochim. Acta* 67, 3773–3783.
- Alexander, C.M.O.D., Fogel, M., Yabuta, H., Cody, G.D., 2007. The origin and evolution of chondrites recorded in the elemental and isotopic compositions of their macromolecular organic matter. *Geochim. Cosmochim. Acta* 71, 4380–4403.
- Alves, L.L. et al., 2012. Capacitively coupled radio-frequency discharges in nitrogen at low pressures. *Plasma Sources Sci. Technol.* 21, 045008.
- Baratta, G.A., Brunetto, R., Leto, G., Palumbo, M.E., Spinella, F., Strazzulla, G., 2008. Raman spectroscopy of ion-irradiated astrophysically relevant materials. *J. Raman Spectrosc.* 39, 211–219.
- Beck, P., Pommerol, A., Thomas, N., Schmitt, B., Moynier, F., 2012. Photometry of meteorites. *Icarus* 218, 364–377.
- Bény-Bassez, C., Rouzaud, J.-N., 1985. Characterization of carbonaceous materials by correlated electron and optical microscopy and Raman microspectroscopy. *Scan. Electron Microsc.*, 119–132.
- Bernard, J.-M., Quirico, E., Brissaud, O., Montagnac, G., Reynard, B., McMillan, P.F., Coll, P., Nguyen, M.-J., Raulin, F., Schmitt, B., 2006. Reflectance spectra and chemical structure of Titan's tholins: Application to the analysis of Cassini-Huygens observations. *Icarus* 185, 301–307.
- Bernard, S., Beyssac, O., Benzerara, K., Findling, N., Tzvetkov, G., Brown Jr., G.E., 2010. XANES, Raman and XRD study of anthracene-based cokes and saccharose-based chars submitted to high-temperature pyrolysis. *Carbon* 48, 2506–2516.
- Bonnet, J.-Y. et al., 2013. Compositional and structural investigation of HCN polymer through high resolution mass spectrometry. *Int. J. Mass Spectrom.* 354–355, 193–203.
- Bradley, J.P., Ishii, H.A., Wozniakiewicz, P., Noguchi, T., Engrand, C., Brownlee, D.E., 2014. Impact of the terrestrial environment on the composition of GEMS. *Lunar Planet. Sci.* 45, Abstract #1777.
- Brucato, J.R., Baratta, G.A., Strazzulla, G., 2006. An infrared study of pure and ion irradiated frozen formamide. *Astron. Astrophys.* 455, 395–399.
- Brunetto, R., Pino, T., Dartois, E., Cao, A.-T., d'Hendecourt, L., Strazzulla, G., Brechignac, P., 2009. Comparison of the Raman spectra of ion irradiated soot and collected extraterrestrial carbon. *Icarus* 200, 323–337.
- Busemann, H., Alexander, C.M.O.D., Nittler, L.R., 2007. Characterization of insoluble organic matter in primitive meteorites by microRaman spectroscopy. *Meteorit. Planet. Sci.* 42, 1387–1416.
- Busemann, H. et al., 2009. Ultra-primitive interplanetary dust particles from the comet 26P/Grigg-Skjellerup dust stream collection. *Earth Planet. Sci. Lett.* 288, 44–57.
- Carrasco, N. et al., 2009. Chemical characterization of Titan's tholins: Solubility, morphology and molecular structure revisited. *J. Phys. Chem.* A113, 11195–11203.
- Cody, G.D. et al., 2011. Establishing a molecular relationship between chondritic and cometary organic solids. *Proc. Natl. Acad. Sci.* 108, 19171–19176.
- Costantini, J.-M., Couvreur, F., Salvetat, J.-P., Bouffard, S., 2002. Micro-Raman study of the carbonization of polyimide induced by swift heavy ion irradiations. *Nucl. Instrum. Meth. B* 194, 132–140.
- Costantini, J.-M., Salvetat, J.-P., Couvreur, F., Bouffard, S., 2005. Carbonization of polyimide induced by swift heavy ion irradiations: Effects of stopping power and velocity. *Nucl. Instrum. Meth. B* 194, 132–140.
- Cottin, H., Fray, N., 2008. Distributed sources in comets. *Space Sci. Rev.* 138, 179–197.
- Dartois, E., Engrand, C., Brunetto, R., Duprat, J., Pino, T., Quirico, E., Rémusat, L., Bardin, N., Briani, G., Mostefaoui, S., Morinaud, G., Crane, B., Szwec, N., Delauche, L., Jamme, F., Sandt, Ch., 2013. Ultracarbonaceous Antarctic micrometeorites, probing the Solar System beyond the nitrogen snow line. *Icarus* 234, 243–252.
- Derenne, S., Coelho, C., Anquetil, C., Szopa, C., Rahman, A.S., McMillan, P.F., Cora, F., Pickard, C.J., Quirico, E., Bonhomme, C., 2012. New insights into the structure and chemistry of Titan's tholins via <sup>13</sup>C and <sup>15</sup>N solid state nuclear magnetic resonance spectroscopy. *Icarus* 221, 844–853.
- Dobrica, E., Engrand, C., Quirico, E., Montagnac, G., Duprat, J., 2011. Raman characterization of carbonaceous matter in CONCORDIA Antarctic micrometeorites. *Meteorit. Planet. Sci.* 46, 1363–1375.

- Ferrari, A.C., Robertson, J., 2000. Interpretation of Raman spectra of disordered and amorphous carbon. *Phys. Rev. B* 61, 14095–14107.
- Ferrari, A.C., Robertson, J., 2001. Resonant Raman spectroscopy of disordered, amorphous, and diamondlike carbon. *Phys. Rev. B* 64, 075414–075514–13.
- Ferrari, A.C., Rodil, S.E., Robertson, J., 2003. Interpretation of infrared and Raman spectra of amorphous carbon nitrides. *Phys. Rev. B* 67, 155306.
- Flynn, G.J., Keller, L.P., Feser, M., Wirick, S., Jacobsen, C., 2003. The origin of organic matter in the solar system: Evidence from the interplanetary dust particles. *Icarus* 67, 4791–4806.
- Fray, N., Bénilan, Y., Cottin, H., Gazeau, M.-C., Minard, R.D., Raulin, F., 2004. Experimental study of the degradation of polymers: Application to the origin of extended sources in cometary atmospheres. *Meteorit. Planet. Sci.* 39, 581–587.
- Fray, N., Bénilan, Y., Biver, N., Bockelée-Morvan, D., Cottin, H., Crovisier, J., Gazeau, M.-C., 2006. Heliocentric evolution of the degradation of polyoxymethylene: Application to the origin of the formaldehyde (H<sub>2</sub>CO) extended source in comet C/1995 O1 (Hale-Bopp). *Icarus* 184, 239–254.
- Hadamcik, E., Renard, J.-B., Alcouffe, G., Cernogora, G., Levasseur-Regourd, A.-C., Szopa, C., 2009. Laboratory light-scattering measurements with Titan's aerosols analogues produced by a dusty plasma. *Planet. Space Sci.* 57, 1631–1641.
- Henning, T., Semenov, D., 2013. Chemistry in protoplanetary disks. *Chem. Rev.* 113, 9016–9042.
- Hewins, 1997. Chondrules. *Annu. Rev. Earth Planet. Sci.* 25, 61–83.
- Hily-Blant, P., Bonal, L., Faure, A., Quirico, E., 2013. The 15N-enrichment in dark clouds and Solar System objects. *Icarus* 223, 582–590.
- Imanaka, H., Khare, B.N., Elsila, J.E., Bakes, E.L.O., McKay, C.P., Cruikshank, D.P., Sugita, S., Matsui, T., Zare, R.N., 2004. Laboratory experiments of Titan tholin formed in cold plasma at various pressures: Implications for nitrogen-containing polycyclic aromatic compounds in Titan haze. *Icarus* 168, 344–366.
- Kerridge, J.F., 1999. Formation and processing of organics in the early Solar System. *Space Sci. Rev.* 90, 275–288.
- Kolokolova, L., Hanner, M.S., Levasseur-Regourd, A.-Ch., Gustafson, 2004. Physical properties of cometary dust from light scattering and thermal emission. In: Festou, M.C. et al. (Eds.), *Comets II*. Univ. of Arizona, Tucson (this volume).
- Krot, A.N. et al., 2009. Origin and chronology of chondritic components: A review. *Geochim. Cosmochim. Acta* 73, 4963–4997.
- Matthews, C.N., Moser, R.E., 1967. Peptide synthesis from hydrogen cyanide and water. *Nature* 215, 1230–1234.
- Mutsukura, N., Akita, K., 1999. Infrared absorption spectroscopy measurements of amorphous CN<sub>x</sub> films prepared in CH<sub>4</sub>/N<sub>2</sub> r.f. discharge. *Thin Solid Films* 349, 115–119.
- Nna-Mvombo, D., de la Fuente, J.L., Ruiz-Bermejo, M., Khare, B., McKay, C.P., 2013. Thermal characterization of Titan's tholins by simultaneous TG-MS, DTA, DSC analysis. *Planet. Space Sci.* 85, 279–288.
- Palumbo, M.E., Ferini, G., Baratta, G.A., 2004. Infrared and Raman spectroscopies of refractory residues left over after ion irradiation of nitrogen-bearing icy mixtures. *Adv. Space Res.* 33, 49–56.
- Pilling, S. et al., 2010. Radiolysis of ammonia-containing ices by energetic, heavy, and highly charged ions inside dense astrophysical environments. *Astron. Astrophys.* 509, A97.
- Quirico, E., Montagnac, G., Lees, V., McMillan, P.F., Szopa, C., Cernogora, G., Rouzaud, J.-N., Simon, P., Bernard, J.-M., Coll, P., Fray, N., Minard, R.D., Raulin, F., Reynard, B., Schmitt, B., 2008. New experimental constraints on composition and structure of tholins. *Icarus* 198, 218–231.
- Quirico, E., Montagnac, G., Rouzaud, J.-N., Bonal, L., Bourot-Denise, M., Duber, S., Reynard, B., 2009. Precursor and metamorphic conditions effects on Raman spectra of poorly-ordered carbonaceous matter in chondrites and coals. *Earth Planet. Sci. Lett.* 287, 185–193.
- Quirico, E., Orthous-daunay, F.-R., Beck, P., Bonal, L., Brunetto, R., Dartois, E., Pino, T., Montagnac, G., Rouzaud, J.-N., Engrand, C., Duprat, J., 2014. Origin of insoluble organic matter in type 1 and 2 chondrites: New clues, new questions. *Geochim. Cosmochim. Acta* 136, 80–99.
- Remusat, L., Palhol, F., Robert, F., Derenne, S., France-Lanord, C., 2006. Enrichment of deuterium in insoluble organic matter from primitive meteorites: A Solar System origin? *Earth Planet. Sci. Lett.* 243, 15–25.
- Robertson, J., Davis, C.A., 1995. Nitrogen doping of tetrahedral amorphous carbon. *Diam. Relat. Mater.* 4, 441–444.
- Rouzaud, J., Oberlin, A., 1990. Structure, microtexture, and optical properties of anthracene and saccharose-based carbons. *Carbon* 27, 517–529.
- Strazzulla, G., Baratta, G.A., Palumbo, M.E., 2001. Vibrational spectroscopy of ion-irradiated ices. *Spectrochim. Acta A* 57, 825–842.
- Szopa, C., Cernogora, G., Boufendi, L., Correia, J., Coll, P., 2006. PAMPRE: A dusty plasma experiment for Titan's tholins production and study. *Planet. Space Sci.* 54, 394–404.
- Thomas, K.L., Blanford, G.E., Keller, L.P., Klock, W., McKay, D.S., 1993. Carbon abundance and silicate mineralogy of anhydrous interplanetary dust particles. *Geochim. Cosmochim. Acta* 57, 1551–1566.
- Vandenbroucke, M., Largeau, C., 2007. Kerogen origin, evolution and structure. *Org. Geochem.* 38, 719–833.
- Vuitton, V. et al., 2010. Ultra high resolution mass spectrometry of HCN polymers and Titan's tholins. *Faraday Discuss.* <http://dx.doi.org/10.1039/C003758C>.
- Yabuta, H. et al., 2012. Coexisting nitrogen-rich and poor organic materials in ultracarbonaceous Antarctic micrometeorite. *Meteorit. Planet. Sci.* (abstract #5196).